

“SOFT–HARD” STRATEGY TO CONSTRUCT A PYRAZINE SULFONIC ACID COPPER(II) SUPRAMOLECULAR STRUCTURE AND A STUDY OF ITS FLUORESCENT PROPERTY

Z. Zheng¹, P. Xu², Y. Jiang³, Y.-J. Liang^{1*},
and J.-X. Li^{4**}

The design and synthesis of functional heterocyclic sulfonic acid polymers would provide much help in studying the coordination behavior, structural optimization, and application of the polymers. In this work, a three-dimensional (3D) supramolecular structure $[\text{Na}_2\text{Cu}(\text{P}-\text{SO}_3)_4]_n$ ($\text{P}-\text{SO}_3\text{H}$ = pyrazine sulfonic acid) is synthesized by a hydrothermal method with the “soft–hard” strategy. The produced polymer is characterized by the elemental analysis, IR spectroscopy, and X-ray crystallography. Crystal diffraction data indicate that the polymer belongs to the $P4/ncc$ space group. Notably, the introduction of a soft alkali metal ion can trigger the specific affinity binding with sulfonate oxygen atoms to give rise to a $\text{Na}-\text{O}-\mu_4$ bridging pattern. The flexible bridging pattern combined with the rigid structure of copper pyrazine sulfonate is likely to be responsible for the production of the final 3D supramolecular structure. Moreover, powder X-ray diffraction data indicated a good phase purity. Thermal stability, Raman features as well as solid-state fluorescent properties are also investigated in detail.

DOI: 10.1134/S0022476621020141

Keywords: heterocyclic sulfonate, coordination chemistry, copper(II) polymer, supramolecular structure, luminescent property.

INTRODUCTION

In recent years, the synthesis and properties of coordination polymers with flexible organic ligands [1-10] have been widely studied, especially those based on heterocyclic sulfonic acid type linkers [11-13]. As a result of its flexible coordination modes, the functional sulfonic acid group with its C_{3v} symmetry may not only easily coordinate metal ions to form layered and interpenetrating structures, but also, by forming bridging patterns, it may also produce extended high-dimensional supramolecular structures. Consequently, many species with novel structures and unique physicochemical properties have been reported [14-16]. As an example, Zhang and co-workers [17] employed the solvothermal self-assembly

¹School of Medical Engineering, Foshan University, Foshan, People's Republic of China; *liangyijun@fosu.edu.cn.

²School of Computer Science of Information Technology, Qiannan Normal University for Nationalities, Duyun, Guizhou, People's Republic of China. ³School of Chemistry and Chemical Pharmaceutical Science, Guangxi Normal University, Guilin, People's Republic of China. ⁴Henan Key Laboratory of Function-Oriented Porous Materials, College of Chemistry and Chemical Engineering, Luoyang Normal University, Luoyang, People's Republic of China; **ljx6281@126.com. Original article submitted August 4, 2020; revised September 16, 2020; accepted September 16, 2020.

strategy to synthesize a Pb(II)-based sulfonate polymer (Pb–BSDC) that these researchers identified as a promising candidate for proton-conduction through interactions of protophilic sulfonic groups and hydrogen bonding. Just recently, Li et al. [18] prepared a series of Cr-based metal-organic frameworks (MOFs) *via* post-synthetic metalation and proved that these novel materials bearing sulfonic acid functional groups would afford the immobilization of catalytically active copper species.

Notably, by applying reasonable design and synthesis strategies, a supramolecular structure can be constructed as part of the process whereby sulfonic acid groups coordinate metal ions [19, 20]. Therefore, a range of molecular interactions, such as hydrogen bonding, π – π weak stacking, and even hydrophobic effects, can be exploited to expand the performance of coordination polymers. In fact, many heterocyclic sulfonic acid-based coordination polymers have been used for micro-sensing, gas adsorption, catalysis, biomedicine, etc., and numerous additional potential applications have been proposed [21–23]. In a previous study, we used pyrazine sulfonic acid as a ligand to synthesize a one-dimensional, rigid, linear Ag(I) coordination polymer that we found to have potential applications in optical sensing [24]. In the case of copper ions, in contrast to other transition metal ions, during polymer construction the existence of a Jahn–Teller effect will significantly affect the d electron cloud distribution and the symmetry of degenerated orbitals during polymer construction, resulting in a variety of distorted coordination configurations [25, 26]. However, due to the lack of research on copper pyrazine sulfonate polymers, the synthesis of these polymers is a challenge, and the performance and applications of such species remain largely unknown. In the present study, a “soft-hard” synthetic strategy was employed to construct a copper-based pyrazine sulfonate polymer $[\text{Na}_2\text{Cu}(\text{P}-\text{SO}_3)_4]_n$ ($\text{P}-\text{SO}_3\text{H}$ = pyrazine sulfonic acid), characterized by a supramolecular structure. Elemental analysis, X-ray crystallography, thermal stability investigations, as well as infrared (IR), Raman, and solid-state fluorescence spectroscopies were used to probe the structure and properties of this polymer. We believe that this study will help to provide a new reference for the construction of functional polymers based on the sulfonate group.

EXPERIMENTAL

Materials. All reagents employed in this study were of analytical grade and were used without further purification. Pyrazine sulfonic acid was synthesized implementing the protocol described in a previous report [27].

Synthesis of $[\text{Na}_2\text{Cu}(\text{P}-\text{SO}_3)_4]_n$. Briefly, the precursor $\text{Cu}(\text{NO}_3)_2 \cdot 3\text{H}_2\text{O}$ (0.4 mmol) was mixed with pyrazine sulfonic acid ($\text{P}-\text{SO}_3\text{H}$, 0.3 mmol) and NaBF_4 (0.1 mmol). The obtained mixture was then added into a mixed solvent containing methanol, THF, and dimethylformamide (DMF) in a specific proportion (2:1:3). Subsequently, the mixture was placed in a 30 mL PETF tank, and it was subjected to a hydrothermal process (140 °C, 72 h). The filtrate thus obtained was allowed to naturally evaporate at room temperature to yield a blue square-like crystal after 47 days. Notably, the crystallization process could be theoretically shortened if the DMF solution was evaporated in vacuum. Yield 5.8% (based on Cu). Anal. calcd for $\text{C}_{16}\text{H}_{12}\text{N}_8\text{Na}_2\text{S}_4\text{CuO}_{12}$ (%): C 25.76, H 1.62, N 15.02; Found (%): C 25.69, H 1.58, N 14.87. IR (KBr, cm^{-1}): 3450 m, 3110 m, 1632 w, 1385 vs, 1265 vs, 1212 vs, 1180 m, 1161 m, 1071 vs, 1037 vs, 845 w, 780 m, 636 vs, 549 w, 508 m.

X-ray crystallography. The X-ray diffraction data on the title compound were collected using an Agilent SuperNova diffractometer at 298 K (MoK_α , $\lambda = 0.071073 \text{ nm}$), and they were analyzed with the Olex2 software [28]. The structure was solved with direct methods and refined using the SHELXTL program package utilizing the full matrix least squares method. In addition, anisotropic thermal parameters were employed for all non-hydrogen atoms [29]. Notably, crystallographic data are listed in Table 1, whereas selected bond distances and angles are reported in Table 2.

Raman spectroscopy. Raman spectroscopy characterization was carried out using an inVia Raman microscope. The $[\text{Na}_2\text{Cu}(\text{P}-\text{SO}_3)_4]_n$ suspension (distilled water, 1 mg/mL) characterized by a range of pH values (i.e., from 3 to 11) were placed in quartz slides for observation. Notably, the 785 nm Argon ion laser with 0.5 mW power was used as an excitation source, and 15 s was the acquisition time for data collection [30].

TABLE 1. Crystal Data and Structure Refinement for $[\text{Na}_2\text{Cu}(\text{P}-\text{SO}_3)_4]_n$

Empirical formula	$\text{C}_{16}\text{H}_{12}\text{N}_8\text{Na}_2\text{S}_4\text{CuO}_{12}$
Formula weight	746.0987
Wavelength, Å	0.71073
Crystal system	Tetragonal
Space group	$P4/ncc$
$a, b, c, \text{\AA}$	13.7007(3), 13.7007(3), 14.9233(5)
$V, \text{\AA}^3$	2801.25(13)
Z	8
Calculated density, g/cm ³	2.204
Absorption coefficient, mm ⁻¹	1.953
$F(000)$	1856
θ , deg	2.97-26.37
Reflections collected	20971
Unique data	1443
R_{int}	0.1046
Completeness to θ , %	99.9
Data / restraints / parameters	1443 / 24 / 130
$GOOF$ on F^2	1.289
Final R indices ($I > 2\sigma(I)$)	$R_1 = 0.0738, wR_2 = 0.1746$
R indices (all data)	$R_1 = 0.0860, wR_2 = 0.1795$
Largest. diff. peak / hole, e/Å ³	2.019 / -0.979

TABLE 2. Bond Distances (Å) and Bond Angles (deg) for $[\text{Na}_2\text{Cu}(\text{P}-\text{SO}_3)_4]_n$

Bond distance		Bond angle	
Cu1–N2 ^{#1}	2.025(7)	N2 ^{#1} –Cu1–N2 ^{#2}	86.1(5)
Cu1–O5	2.101(4)	O1–Na1–O1 ^{#5}	164.1(3)
Cu1–N1 ^{#3}	2.058(7)	O1 ^{#5} –Na1–O1 ^{#6}	91.09(4)
Na1–O1 ^{#4}	2.427(7)	O1 ^{#5} –Na1–O4 ^{#5}	80.4(4)
Na1–O4 ^{#5}	2.93(2)	O4 ^{#5} –Na1–O4 ^{#4}	154.8(5)
Na2–O7 ^{#8}	2.78(8)	O1–Na1–O4 ^{#6}	80.1(4)
O5–Na2 ^{#9}	2.92(4)	N2 ^{#2} –Cu1–O3	90.6(3)
Cu1–N1	2.058(7)	N2 ^{#1} –Cu1–O3 ^{#3}	90.6(3)
Cu1–O3 ^{#3}	2.262(6)	N1–Cu1–O3 ^{#3}	88.2(3)
Na1–O1 ^{#6}	2.427(7)	O1 ^{#4} –Na1–O1 ^{#6}	164.1(3)
Na1–O4 ^{#4}	2.93(2)	O1–Na1–O4 ^{#5}	84.5(4)
Na2–O2 ^{#7}	2.543(7)	O1 ^{#6} –Na1–O4 ^{#5}	80.1(4)
Na2–O5 ^{#9}	2.92(4)		

Symmetry transformations used to generate equivalent atoms: ^{#1} $x-1/2, -y+1, -z+3/2;$ ^{#2} $y, -x+3/2, z;$ ^{#3} $-y+1, -x+1, -z+3/2;$ ^{#4} $-y+1, x-1/2, -z+1;$ ^{#5} $-x+3/2, -y+1/2, z;$ ^{#6} $y+1/2, -x+1, -z+1;$ ^{#7} $-y+3/2, x, z;$ ^{#8} $x+1/2, -y+1, -z+3/2;$ ^{#9} $-y+1, x+1/2, -z+1$

RESULTS AND DISCUSSION

Structural description. Single crystal X-ray crystallography data suggested that the copper ion was coordinated by four adjacent pyrazine sulfonate anionic ($\text{P}-\text{SO}_3$) ligands to produce a distorted octahedral configuration with central symmetry (Fig. 1a). The nitrogen atoms on four pyrazine rings coordinated the copper ion to form the equatorial plane,

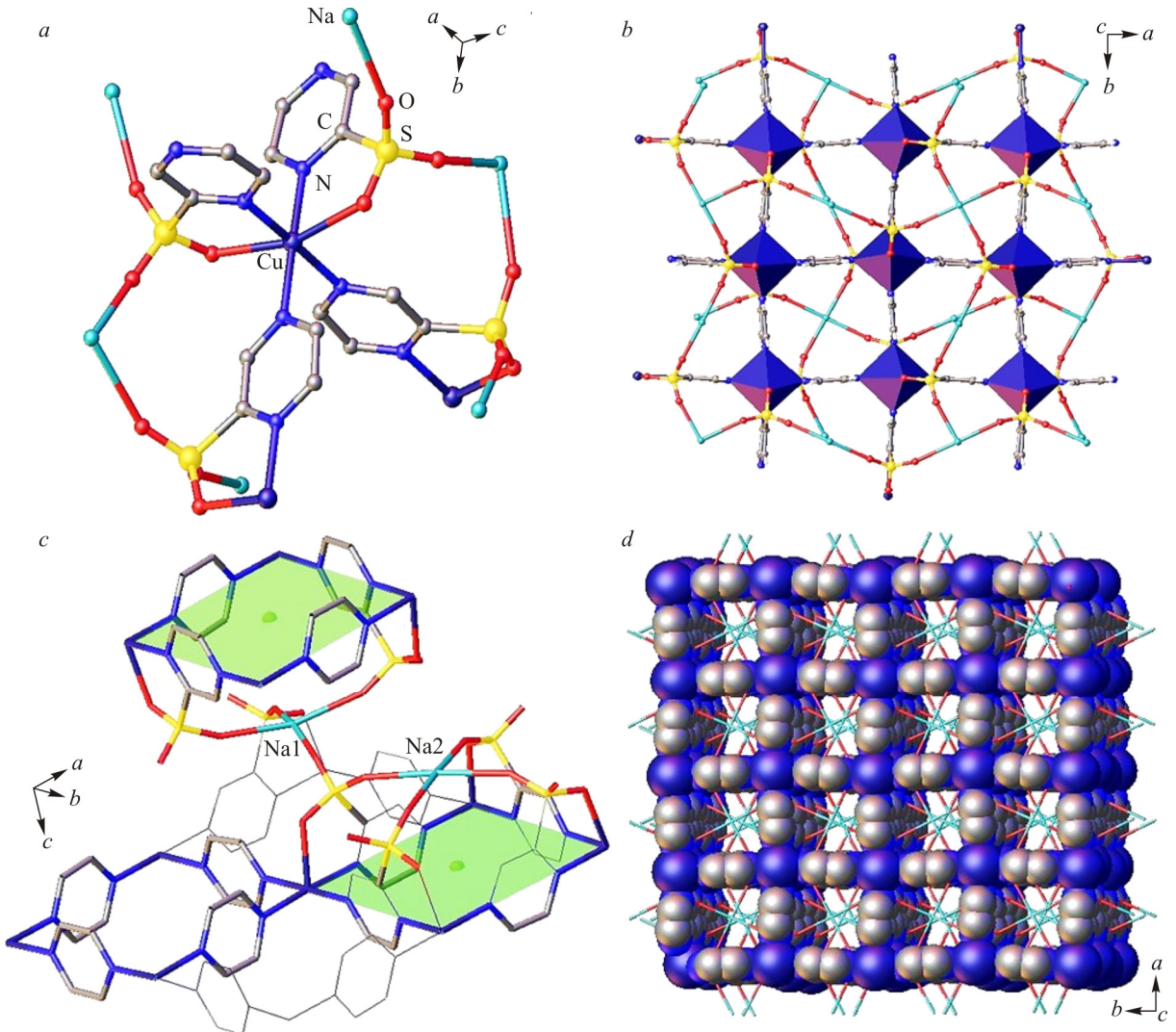


Fig. 1. Crystal structure of $[Na_2Cu(P-SO_3)_4]_n$ ($P-SO_3H$); coordination environment of the Cu(II) ion (a); 2D framework with a shape of a regular square lattice (b); Na–O- μ_4 bridging pattern of $[Na_2Cu(P-SO_3)_4]_n$ (c); 3D supramolecular structure produced as a consequence of the Na–O bridging effect (d).

whereby the axial positions were filled by sulfonate oxygen atoms of adjacent ligands ($Cu1-O$ 2.262 Å; $Cu1-N1$ 2.058 Å; $Cu1-N2$ 2.025 Å). In detail, two $P-SO_3$ anions coordinated the copper ion in a bidentate chelate fashion *via* the oxygen and nitrogen atoms in an inverted form, whereas the other two $P-SO_3$ anions coordinated the metal center through their nitrogen atoms to produce a two-dimensional (2D) framework. The size of the framework unit was found to be 6.86×6.86 Å (Fig. 1b). In particular, based on the obtained crystal configuration, we speculated that in the octahedral potential energy field formed by copper ions, the electron configuration of the d orbital splitting should be $(T_{2g})^6(d_z^2)^2(d_{x^2-y^2})^1$. The resulting structure could effectively reduce the repulsive forces of the ligands on the x and y axes, thereby causing the $P-SO_3$ ligands on the equatorial plane to move closer to the metal center and prompting the electrons on the d_z^2 orbital to move outward. Consequently, the energy level of the $d_{x^2-y^2}$ orbital will increase, whereas that of the d_z^2 orbital will decrease, resulting in the Cu–N bonds in the xy plane being much shorter than the Cu–O bonds perpendicular to the surface (z axis). The obtained stretched octahedral configuration is the result of distortions caused by the Jahn–Teller effect. The energy of the entire system is reduced by effectively eliminating the degeneracy of the e_g energy level, an outcome that is beneficial to the stability of the structure [25, 31]. Moreover, as clearly evinced from Fig. 1c, sodium ions were coordinated by two sulfonic oxygen atoms in

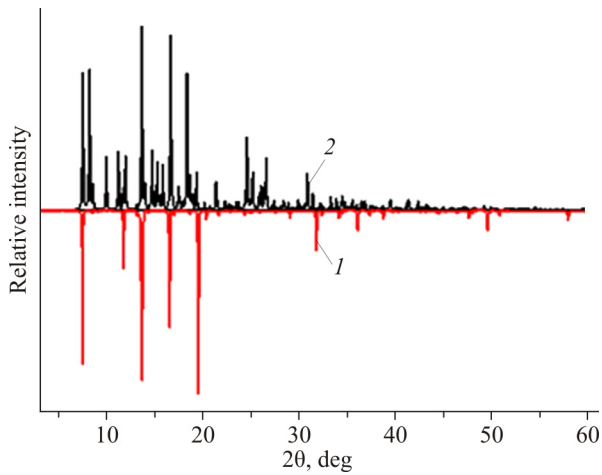


Fig. 2. Experimental (1) and simulated (2) PXRD patterns of $[Na_2Cu(P-SO_3)_4]_n$.

terms of affinity, so that two kinds of Na–O- μ_4 bridging configurations ($Na1-O$, 2.427 Å, $O1-Na1-O1^{#6}$, 91.09°; $Na2-O$, 2.543 Å, $O2-Na2-O2^{#2}$, 90°) were produced. Apparently, these two Na–O- μ_4 bridging patterns play different roles, so that the copper sulfonate frame acts as a layer, whereas the flexible sodium sulfonate frames function as pillars of the 3D supramolecular structure (Fig. 1d).

Powder X-ray diffraction. As can be evinced from Fig. 2, a few of the peaks in the experimental power X-ray diffraction (PXRD) pattern of the polymer are observed to be in different positions compared with their counterparts of the simulated pattern. We believe that the following explanations may account for the described phenomenon: (i) the simulated pattern was constructed after absorption data correction based on the single crystal data, whereas the obtained PXRD experimental data were not corrected for absorption; (ii) incomplete exposure of the diffraction peaks may be a reason for the preferred orientation of the crystal, in other words, the crystal does not fully expose all crystal faces; (iii) many defects are present on the surface of the as-synthesized crystals, so that most X-rays are absorbed by the samples instead of being scattered.

Thermal analysis. Investigation of the thermal stability of $[Na_2Cu(P-SO_3)_4]_n$ will provide some information that could help to expand the applications of this polymer. Herein, the thermogravimetric analysis of the polymer was performed applying a heating rate of 15 °C/min from ambient temperatures to 800 °C. As can be evinced from Fig. 3, the first weight loss was observed at ~227 °C, and it was attributed to the release of guest molecules (Obs. 5.3%, Calcd 4.9%). Later on, an obvious inflection point appeared, and the framework rapidly decomposed on continuous heating, until the maximum

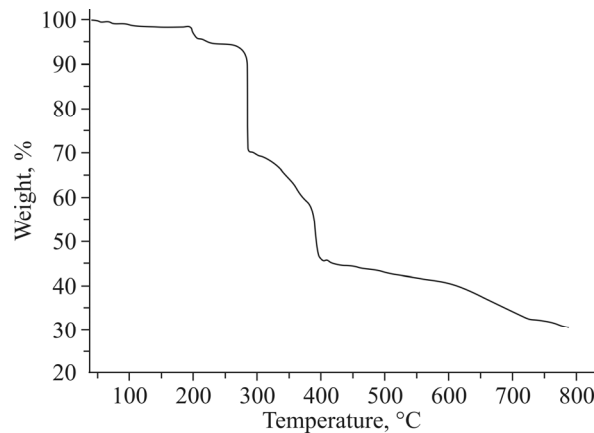


Fig. 3. Thermogravimetric curve obtained for $[Na_2Cu(P-SO_3)_4]_n$.

weight loss was observed to occur at 397 °C (Obs. 46.8%, Calcd 47.4%). The polymer degradation rate slowed down as the temperature kept increasing, until the pyrolysis residue formed at ~800 °C (Obs. 29.6%, Calcd 28.3%).

Raman spectroscopy. It should be known that copper(II) sulfonate complexes with potential anticancer and antibacterial activities can be found in the literature [32, 33]. In this regard, we supposed that the use of Raman spectroscopy to explore the stability of the crystal structure under different pH conditions would be particularly important, which may provide a valuable reference for achieving biomedical application of pyrazine sulfonic acid-based copper (II) complexes in the future. The Raman spectroscopic features of the $[\text{Na}_2\text{Cu}(\text{P}-\text{SO}_3)_4]_n$ suspension (distilled water, 1 mg/mL) characterized by different pH values are illustrated in Fig. 4. The peaks at $\sim 800 \text{ cm}^{-1}$ and $\sim 700 \text{ cm}^{-1}$ were assigned to the bending vibration of the S–C bond and the asymmetric vibration of the S=O bond of the sulfonate ligand, respectively. The signal near 550 cm^{-1} was attributed to the bending vibration of the S–C bond in the ligand. The peaks appearing in the range 250–400 cm^{-1} were attributed to bending vibrations of Cu–O and Cu–N bonds. As the solution pH gradually increased, few Raman signals were observed until pH ~ 11. To our knowledge, Raman spectroscopy may provide information on the crystallinity of the sample, the presence of structural defects, and even the microstructural features of the sample [30]. Therefore, the variation of signals resulting from metal coordination was ascribed to the bending vibration, which may be induced by a low proton concentration ($\text{pH} > 3$) [34, 35]. In any event, the described phenomenon should be the subject of additional analyses and verifications.

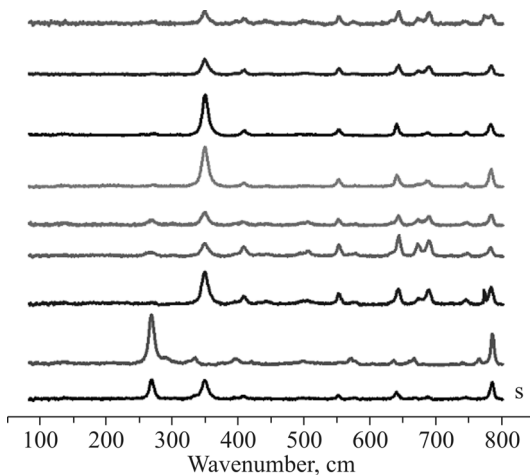


Fig. 4. Raman spectra of $[\text{Na}_2\text{Cu}(\text{P}-\text{SO}_3)_4]_n$ solutions characterized by various pH values: 3, 4, 5, 6, 8, 9, 10, 11 down up.

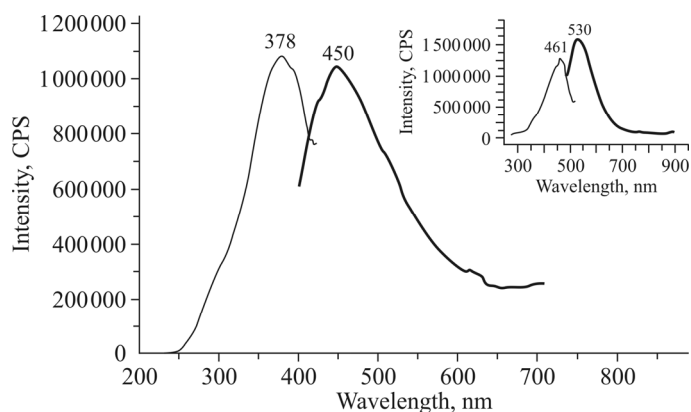


Fig. 5. Solid-state photoluminescence spectra of $[\text{Na}_2\text{Cu}(\text{P}-\text{SO}_3)_4]_n$ (inset depicts solid-state photoluminescence spectra of P-SO₃H [24]).

Luminescence. In order to explore the luminescent properties of pyrazine sulfonate-related polymers, the fluorescence spectra of $[\text{Na}_2\text{Cu}(\text{P}-\text{SO}_3)_4]_n$ and the ligand were recorded at room temperature. The maximum emission signal of the polymer was detected at 450 nm, at an excitation wavelength of 378 nm (Fig. 5). Notably, the fluorescence peaks of the ligand were more intense than those of the polymer, and they underwent a ~ 80 nm red shift ($\lambda_{\text{ex}} = 461$ nm, $\lambda_{\text{em}} = 530$ nm), which can be attributed to the fact that the coordination of Cu^{2+} and Na^+ ions might increase the conjugation effect in the ligand. Therefore, part of the fluorescence energy of the ligand would be transferred to the metal ion through the sulfonate moiety, which would in turn result in a certain degree of fluorescence quenching in the polymer [36, 37].

CONCLUSIONS

In summary, by employing a “soft–hard” strategy, the pyrazine sulfonate polymer $[\text{Na}_2\text{C}(\text{P}-\text{SO}_3)_4]_n$, which displays a supramolecular structure, was successfully synthesized *via* the hydrothermal method. Taking advantage of the Jahn–Teller effect, the symmetry and orbital degeneracy of copper ions can be effectively reduced, thus causing a reduction of the energy of the system. Evidence suggests that, as a result of the unique planar symmetric rigid features of the pyrazine ring which at the same time coordinated with metal ions, the 2D layered arrangement might be the dominant structural feature. However, the introduction of alkali metal that can form a bond with the oxygen atom of the sulfonate moiety showed a specific affinity. The softer sodium ion acted as a good proton conductor and a bridge channel to expand the 3D structure of the polymer, which provides a good reference for constructing functional sulfonate polymers with diverse configurations in the future.

FUNDING

The research was supported by the Key scientific research projects in Colleges and Universities of Henan province (No. 21A150036), the science and technology key project of Covid-19 in Foshan city (No. 2020001000206), the Basic and Applied Basic Research Foundation of Guangdong Province (No. 2020131515120033), and the Scientific Research Program of High-Level Talents of Foshan University (No. CGZ07001).

ADDITIONAL INFORMATION

Author contributions. Zhaoguang Zheng: manuscript written. Peng Xu and Yimin Jiang: performed the experiments and participated in discussion of the results. Yi-Jun Liang and Junxia Li: supervision and revision of the manuscript. All authors have given approval to the final version of the manuscript.

Crystallographic data for the structural analysis have been deposited with the Cambridge Crystallographic Data Center under a CCDC deposition number 1997776 for $[\text{Na}_2\text{Cu}(\text{P}-\text{SO}_3)_4]_n$. Copies of this information may be obtained free of charge from the CCDC, 12 Union Road, Cambridge, CB2 1EZ, UK (Fax: +44 1223 336 033; E-mail: deposit@ccdc.cam.ac.uk or www.ccdc.cam.ac.uk).

CONFLICT OF INTERESTS

The authors declare that they have no conflict of interests.

REFERENCES

1. Y.-J. Liang, G. Feng, X. Zhang, J.-X. Li, and Y. Jiang. *J. Struct. Chem.*, **2021**, *62*(2), 316.
2. Z. X. Du and J. X. Li. *Z. Naturforsch.*, **2020**, *75b*(6–7), 577.
3. J. X. Li, Z. X. Du, Q. Y. Pan, L. L. Zhang, and D. L. Liu. *Inorg. Chim. Acta*, **2020**, *509*, 119677.
4. J. X. Li, Z. X. Du, L. Y. Xiong, L. L. Fu, and W. B. Bo. *J. Solid State Chem.*, **2021**, *293*, 121799.

5. J. X. Li, Z. X. Du, L. L. Zhang, D. L. Liu, and Q. Y. Pan. *Inorg. Chim. Acta*, **2020**, *512*, 119890.
6. Z. X. Du and J. X. Li. *Z. Krisallogr. NCS*, **2015**, *230*, 321.
7. J. X. Li, Z. X. Du, J. Wang, and X. Feng,. *Z. Naturforsch.*, **2019**, *74*(11–12)b, 839.
8. Z. X. Du and J. X. Li. *Inorg. Chim. Acta*, **2015**, *436*, 159.
9. J. X. Li, Z. X. Du, and W. P. Huang. *Synth. React. Inorg. Met. Chem.*, **2014**, *44*, 352.
10. J. X. Li and Z. X. Du. *J. Coord. Chem.*, **2016**, *69*, 2563.
11. P. Thuéry, Y. Atoini, and J. Harrowfield. *Dalton Trans.*, **2019**, *48*, 8756.
12. A. G. Mahmoud, L. M. Martins, M. F. C. Silva, and A. J. L. Pombeiro. *Catalysts*, **2019**, *9*, 611.
13. D. K. Maity, S. Ghosh, K. Otake, H. Kitagawa, and D. Ghoshal. *Inorg. Chem.*, **2019**, *58*, 12943.
14. P. M. Shanthi, P. J. Hanumantha, K. Ramalinga, B. Gattu, M. K. Datta, and P. N. Kumta. *J. Electrochem. Soc.*, **2019**, *166*, A1827.
15. M. M. Islam, P. Bhanja, M. Halder, A. Das, A. Bhaumik, and I. S. Manirul. *Mol. Catal.*, **2019**, *475*, 110489.
16. S. Xu, X. Li, Y. Wang, Z. Hu, and R. Wang. *J. Appl. Polym. Sci.*, **2019**, *136*, 47178.
17. H. Zhang, Z. A. Yan, Z. M. Wu, Z. Q. Lin, W. M. Liao, and J. He. *J. Solid State Chem.*, **2020**, *287*, 121325.
18. X. Li, Z. Zhou, Y. Zhao, D. Ramella, and Y. Luan. *Appl. Organomet. Chem.*, **2020**, *34*, e5445.
19. D. V. Hardouin, C. Dimeck, and F. Schaper. *Can. J. Chem.*, **2019**, *97*, 178.
20. M. Bouhdada, M. E. L. Amane, and N. El Hamzaoui. *Inorg. Chem. Commun.*, **2019**, *101*, 32.
21. M. L. Sall, A. K. D. Diaw, D. Gningue-Sall, A. Chevillot-Biraud, N. Oturan, M. A. Oturan, and J. J. Aaron. *Environ. Sci. Pollut. Res.*, **2017**, *24*, 21111.
22. S. Chen, J. Li, W. Li, X. Z. Guo, and Y. Zhao. *J. Solid State Chem.*, **2019**, *277*, 510.
23. M. Lo, A. K. D. Diaw, D. Gningue-Sall, M. A. Oturan, M. M. Chehimi, and J. J. Aaron. *Luminescence*, **2019**, *34*, 489.
24. Y. Liang, X. Meng, F. Huang, J. J. Guo, and Y. M. Jiang. *J. Coord. Chem.*, **2011**, *64*, 3751.
25. B. Murphy and B. Hathaway. *Coord. Chem. Rev.*, **2003**, *243*, 237.
26. J. Conradie. *Inorg. Chim. Acta*, **2019**, *486*, 193.
27. S. Fujii, T. Takagi, and M. Seki. *Agric. Biol. Chem.*, **1982**, *46*, 2169.
28. O. V. Dolomanov, L. J. Bourhis, R. J. Gildea, J. A. K. Howard, and H. Puschmann. *J. Appl. Crystallogr.*, **2009**, *42*, 339.
29. G. M. Sheldrick. *SHELXS-97*, Program for Crystal Structure Solution. **1997**.
30. Y. J. Liang, Y. Zhang, Z. Guo, J. Xie, T. Bai, J. Zou, and N. Gu. *Chem. Eur. J.*, **2016**, *22*, 11807.
31. T. Z. Forbes and S. C. Sevov. *Inorg. Chem.*, **2009**, *48*, 6873.
32. S. Wahid, M. Hanif, S. Jahangir, M. Shafique, H. A. Shahid, H. Muhammad, S. A .A. Shah, M. A. Versiani, K. M. Khan, and I. A. Tahiri. *J. Mol. Struct.*, **2019**, *1184*, 569.
33. W. L. Leong and J. J. Vittal. *J. Inclusion Phenom. Macrocyclic Chem.*, **2011**, *71*, 557.
34. A. A. McConnell, J. A. Nimmo, and W. E. Smith. *J. Raman Spectrosc.*, **1989**, *20*, 375.
35. S. Hashimoto, S. Ohsaka, H. Takeuchi, I. Harada. *J. Am. Chem. Soc.*, **1989**, *111*, 8926.
36. S. Ressalan and C. S. P. Iyer. *J. Lumin.*, **2005**, *111*, 121.
37. X. Zhang, G. Y. Dong, B. Yu, K. Van-Hecke, and G. H. Cui. *Transition Met. Chem.*, **2015**, *40*, 907.